# Photographic Text-to-Image Synthesis with a Hierarchically-nested Adversarial Network

Anonymous CVPR submission

Paper ID 2823

## Abstract

*This paper presents a novel method to deal with the challenging task of generating images conditioning on semantic image descriptions. We propose an effective end-to-end single-stream network that can generate photographic high-resolution images. Our method leverages deep representations of convolutional layers and introduces accompanying hierarchical-nested adversarial games inside the network hierarchy, which regularize intermediate representations and assist training to capture the complex image statistics. We present an extensile network architecture to cooperate with discriminators and push generated images to high resolutions. We adopt a multi-purpose adversarial training strategy at multiple nested side outputs to encourage more effective image-text alignment in order to improve the semantic consistency and image fidelity simultaneously. Furthermore, we introduce a new visual-semantic similarity measure to evaluate the semantic consistency of generated images, thus alleviates the needs of human evaluation. With extensive experimental validation on three public datasets, our method significantly improves previous state of the arts on all datasets over different evaluation metrics (e.g. a* 11.86 *Inception score on COCO).*

## 1. Introduction

Photographic text-to-image synthesis is a significant problem in generative model research [33], which aims to learn a mapping from one semantic text space to one complex RGB image space. This task requires the generated images to be not only realistic but also *semantically consistent*, i.e., the generated images not only preserve object color and sketch in descriptions but also fine-grained descriptive details in image pixels.

Generative adversarial networks (GANs) have become the main solution to this task. Reed *et al*. [33] address this task through a GAN based framework. But this method only scale up to $64^2$ resolution and can barely generate vivid object details. Based on this method, StackGAN [42] propose a two-stage training strategy, which stacks another low-to-high resolution GAN to generate high-resolution $256^2$ images. Later on, [8] proposes to bypass the difficult of learning mappings from vector embeddings to RGB images and treat it as a pixel-to-pixel translation problem [15]. It works by re-rendering an arbitrary-style $128^2$ training image conditioned on a targeting description. However, its high-resolution synthesis capability remains unclear. At present, training a generative model to map from a low-dimensional text space to a high-resolution and diverse image space in a fully end-to-end manner still remains unsolved.

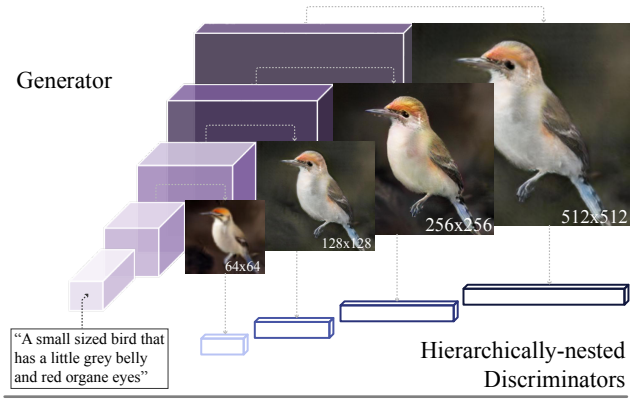


This little bird has a white breast and belly, with a gray crown and black secondaries.

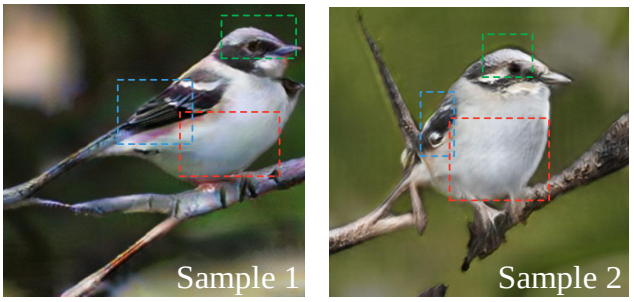


Figure 1: Top: Overview of our hierarchically-nested adversarial network. Bottom: Two generated results where fine-grained details are highlighted.

Text-to-image synthesis using GANs has two major difficulties. The first is balancing the convergence between generators and discriminators [11, 36], which is actually a long-term problem in GANs. The second is stably modeling the huge pixel space in high-resolution images [42]. An effective strategy to regularize generators is critical to help capture the complex image statistics [13] as well as guarantee semantic consistency.

With careful consideration of these problems, in this paper, we propose a novel end-to-end method that can directly model high-resolution image statistics and generate semantically consistent and photographic image (see Figure 1). The contributions are described as follows.

Our generator resembles a simple vanilla GAN, without requiring any multiple internal text conditioning like [42] or outside image annotation supervision like [6]. To tackle the problem of the big leap from the text space to the high-resolution image space, our insight is to leverage and regularize hierarchical representations with additional deep adversarial constraints. We introduce accompanying hierarchically-nested discriminators at multi-scale intermediate layers to play adversarial games and thereby encourage the generator approaching the real training data distribution. We also propose a new convolutional neural network (CNN) for generator to support connections of discriminators at side outputs more effectively. To guarantee the image diversity and semantic consistency, we enforce nested discriminators at different hierarchies to simultaneously differentiate real-and-fake image-text pairs as well as real-and-fake global images or local image patches.

We validate our proposed method on three datasets, CUB birds [39], Oxford-102 flowers [29], and large-scale MSCOCO [23]. In complement of existing evaluation metric (inception score [36]) for generative models, we also introduce a new visual-semantic similarity metric to evaluate the alignment between generated images and conditioned text. Extensive experimental results and analysis demonstrate the effectiveness of our method and significantly improved performance compared against previous state of the arts on three metrics. All source code will be released.

## 2. Related Work

We discussed related work and further clarify the novelty of our method by comparing with them.

Deep generative models have attracted wide interests recently, including GANs [11], Variational Auto-encoders (VAE) [18], etc [31]. There are substantial existing methods investigating better usage of GANs for different applications, such as image synthesis [32, 37], (unpaired) pixel-to-pixel translation [15, 44], medical applications [5], etc [21, 13].

Text-to-image synthesis is attractive problem in GANs. Reed *et al*. [33] is the first to introduce a method that can generate $64^2$ resolution images, which is similar with DCGAN [32]. This method presents a new strategy for image-text matching aware adversarial training. Reed *et al*. [34] propose generative adversarial what-where network (GAWWN) to enable location and content instructions in text-to-image synthesis. StackGAN *et al*. [42] propose a two-stage stacking GAN training approach that is able to generate $256^2$ compelling images. Recently, Dong *et al*. [8] propose to learn a joint embedding of images and text so as to re-render a prototype image conditioned on a targeting description. Cha *et al*. [27] explore the usage of the perceptional loss with a CNN pretrained on ImageNet [16] and Dash *et al*. [6] make use of auxiliary classifiers (similar with [30]) to assist GAN training for text-to-image synthesis.

Learning a continuous mapping from a low-dimensional embedding manifold to a complex real data distribution is a long-standing problem. Although GANs have made significant progress, there are still many unsolved difficulties, e.g. training instability and high-resolution generation. Wide methods have been proposed to address the training instability, such as various training techniques [35, 1, 2, 37, 30], regularization using extra knowledge (e.g. image labels, ImageNet CNNs, etc) [9, 21, 6, 6], or different generator and discriminator combinations [26, 10, 41, 13]. *While our method shows a new way to unite generators and discriminators and does not requires any extra knowledge apart from training paired text and images.* Additionally, it is easy to see the training difficulty increases significantly as targeting image resolution increases.

To synthesize high-resolution images, cascade networks are effective to decompose originally difficult tasks to multiple subtasks (Figure 2 A). Denton *et al*. [7] train a cascade of GANs in a Laplacian pyramid framework (LAPGAN) and use each to synthesis details and push up the output resolution through by-stage refinement. StackGAN also shares some similar idea with LAPGAN. Inspired by this strategy, Chen *et al*. [4] present a cascaded refinement network to synthesize high-resolution scene from semantic maps. Recently, Karras *et al*. [17] propose a progressive training of GANs for high-resolution image generation (Figure 2 C). *Compared with these strategies that train low-to-high resolution GANs progressively, our method has the advantages of leveraging mid-level representations to encourage implicit subtask integration, which makes end-to-end high-resolution image synthesis in a single vanilla-like GAN possible.*

Leveraging hierarchical representations of neural networks is an effective way to enhance implicit multi-scaling and ensembling for tasks such as image recognition [22] and pixel or object classification [40, 3, 25]. Particularly, using deep supervision [22] in hierarchical convolutional layers can increase the discriminativeness of feature representations. *Our hierarchically-nested adversarial objective*

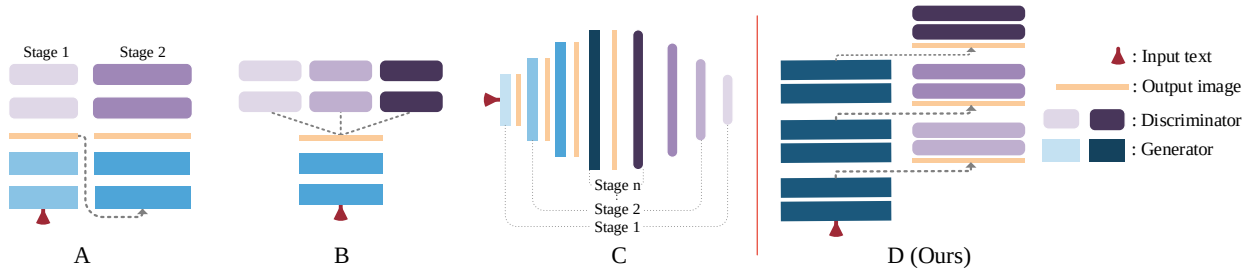


Figure 2: Overviews of some typical GAN frameworks. **A** uses multi-stage GANs [42, 7]. **B** uses multiple discriminators with one generator [10, 28]. **C** progressively trains symmetric discriminators and generators [17, 13]. **A** and **C** can be viewed as decomposing high-resolution tasks to multi-stage low-to-high resolution tasks. **D** is our proposed framework that uses a single-stream generator with hierarchically-nested discriminators trained end-to-end.

*is inspired by these families of deeply-supervised CNNs.*

## 3. Method

### 3.1. Adversarial objective basics

In brief, the two-player game in GANs [11] is played by a generator $G$ network and a discriminator $D$ network, which are alternatively trained to compete with each other and thereby improve each other. The discriminator is optimized to distinguish synthesized images from real images, meanwhile, the generator is trained to generate fake images to fool the discriminator. Concretely, the overall min-max optimization objective is defined as:

$$G^*, D^* = \arg \min_G \max_D \mathcal{V}(D, G, Y, \boldsymbol{z}), \tag{1}$$

where $Y$ denotes training images and $\boldsymbol{z} \sim \mathcal{N}(0, 1)$ denotes a random noise. The value function $\mathcal{V}$ aims to minimize the Jensen-Shannon divergence between the data and the model distribution. $G$ is learned to approximate $G(\boldsymbol{z}) \sim p(Y)$. The loss $\mathcal{L}$ for the valuation function is usually a cross-entropy loss, such that $\mathcal{V}(\cdot) = -\mathcal{L}(\cdot)$.

### 3.2. Hierarchical-nested adversarial objectives

Numerous methods have demonstrated ways to unite generators and discriminators for image synthesis. Figure 2 and Section 2 discuss some typical frameworks. Our method actually explores a new dimension of playing this adversarial game along the depth of a CNN (Figure 2 D), which integrates additional discriminators at mid-level features of the generator $\mathcal{G}$. The hierarchically-nested objectives act as regularizers to the hidden space of $\mathcal{G}$, which can reduce the training instability and also offer a short path for better error signal flows.

The proposed $\mathcal{G}$ is a CNN (defined in Section 3.4) with multiple side outputs:

$$X_1, ..., X_s = \mathcal{G}(\boldsymbol{t}, \boldsymbol{z}), \tag{2}$$

where $\boldsymbol{t} \sim p(data)$ denotes a sentence embedding vector in the real training data distribution (generated by a text character encoder). $\mathcal{G}$ produces $s - 1$ side outputs $\{X_1, ..., X_{s-1}\}$ (resolution-growing images) and a final output $X_s$ with the highest resolution.

For each $X_i$, we propose to apply a distinct discriminator $D_i$ to perform adversarial games independently. Therefore, our full min-max objective is defined as

$$\mathcal{G}^*, \mathcal{D}^* = \arg \min_G \max_{\mathcal{D}} \mathcal{V}(\mathcal{G}, \mathcal{D}, \mathcal{Y}, \boldsymbol{t}, \boldsymbol{z}), \tag{3}$$

where $\mathcal{D} = \{D_1, ..., D_s\}$, and $\mathcal{Y} = \{Y_1, ..., Y_s\}$ denotes a set of training images at multi-scales, $\{1, ..., s\}$. Compared with Eq. (1), one generator competes with multiple discriminators $\{D_i\}$ at different hierarchies (Figure 2 D), which learns diverse discriminative features in different contextual scales, respectively.

In principle, the lower-resolution side output is forced to learn semantic consistent image structures (e.g., object sketch, color, and background), and the subsequent higher-resolution side outputs are used to render details on these image structures. Since our method is able to be trained in an end-to-end fashion, the lower-resolution outputs can fully enjoy top-down knowledge from discriminators for higher resolutions, such that consistent image structures and styles appear in both low and high resolutions. As an evidence, we can obtain significantly more consistent results exhibited in both low- and high-resolution outputs than StackGAN (see experiments). According to our empirical observation, our design is able to reduce the model instability, especially at the early stage of the training.

### 3.3. Multi-purpose adversarial losses

Our generator produces size-growing side outputs which compose an image pyramid. We leverage this hierarchy property and allow adversarial losses to be multi-purpose to capture different (conditioned and unconditioned) statistics, with a goal to guarantee both semantic consistency and image fidelity.

To guarantee semantic consistency, we adopt the matching-aware pair loss proposed by [33]. The discriminator is designed to take image-text pairs as inputs and trained

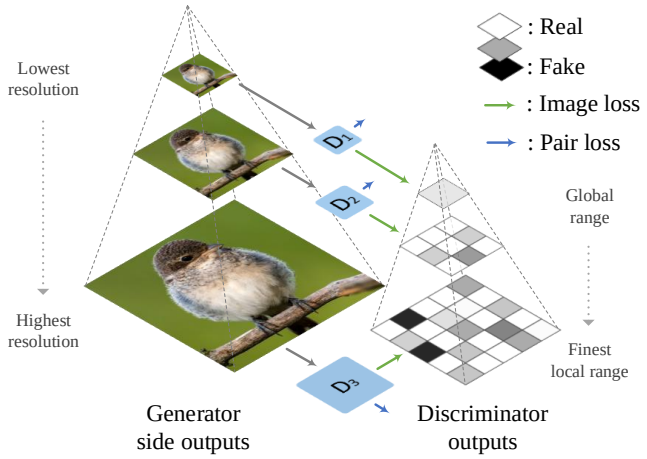


Figure 3: Given a set of images from the side output pyramid of the generator, the corresponding discriminator $D_i$ computes the matching-aware pair loss and adaptive local image loss (outputting a $R\times R$ probability map to classify real or fake patches). The focal range decreases as the image size grows.

to identify two types of errors: real image with mismatched text and fake image with conditioned text.

The pair loss is designed to guarantee the global semantic consistency. However, there lacks an explicit loss that forces the discriminator to differentiate pure real images from fake images. Combining both tasks (generating realistic images and matching image styles with text) into one loss complicates the already challenging learning tasks. Moreover, as the image resolution goes higher, it might be challenging for a global pair-loss discriminator to capture the local fine-grained details. In addition, as pointed in [37], a single global discriminator may over-emphasize certain biased local features and lead to artifacts.

To guarantee the image fidelity, our solution is to add local adversarial image losses on image patches. We expect the low-resolution discriminator to focus on global structures, while high-resolution outputs focus more on local image details. Through the pyramid of the size-growing side outputs, we configure the size of each image patch need to classify, termed the focal range, to be adaptive. The local image adversarial loss can be implemented as an fully CNN [37, 44], and it is the second branch of our discriminator for the pair loss (see Section 3.4). Figure 3 illustrates how hierarchically-nested discriminators compute the two losses on generated image in the pyramid.

**Full Objective** Overall, our hierarchically-nested discriminators $\{D_i\}$ minimize the following loss[1]:

$$\mathcal{L}(\mathcal{G},\mathcal{D}) = \sum_{i=1}^{s} \Big( L_2\big(D_i(Y_i)\big) + L_2\big(D_i(Y_i,\boldsymbol{t}_Y)\big) + \overline{L_2}\big(D_i(X_i)\big) + \overline{L_2}\big(D_i(X_i,\boldsymbol{t}_{X_i})\big) + \overline{L_2}\big(D_i(Y_i,\boldsymbol{t}_{\overline{Y}})\big)\Big), \tag{4}$$

where $L_2(x) = \mathbb{E}\big[(x-\mathbb{I})^2\big]$ is the mean-square loss (instead of the conventional cross-entropy loss) and $\overline{L_2}(x) = \mathbb{E}\big[x^2\big]$. For local image loss with varying focal ranges, the shape of $x, \mathbb{I} \in \mathbb{R}^{R\times R}$ varies accordingly (see Figure 3). $R = 1$ refers to the (largest local) global range. $D_i(X_i)$ denotes the image loss branch and $D_i(X_i,\boldsymbol{t}_{X_i})$ denotes the pair loss branch (conditioned on $\boldsymbol{t}$). $\{Y_i,\boldsymbol{t}_Y\}$ denotes a matched image-text pair and $\{Y_i,\boldsymbol{t}_{\overline{Y}}\}$ denotes a mismatched image-text pair.

Furthermore, this separation of the image loss from the matching loss in our method opens further possibilities, such as utilizing the unlabeled image to improve both the generator and discriminator. In the spirit of variational auto-encoder [19] and the practice of StackGAN [42], namely conditioning augmentation (CA), we sample the input text $\boldsymbol{t}$ from a Ganssian distribution $\mathcal{N}(\mu(\boldsymbol{t}),\Sigma(\boldsymbol{t}))$, where $\mu$ and $\Sigma$ are functions of $\boldsymbol{t}$ (learned with the network), which produces a 256-d text input. We add the Kullback-Leibler divergence regularization term, $D_{KL}(\mathcal{N}(\mu(\boldsymbol{t}),\Sigma(\boldsymbol{t}))||\mathcal{N}(0,\boldsymbol{I}))$ [19], to the $G$ loss to force the smooth sampling over the text embedding distribution.

### 3.4. Architecture Design

**Generator** The generator is simply composed by three kinds of modules, termed as $K$-repeat res-blocks, stretching layers, and linear compression layers. A single res-block in the $K$-repeat res-block is a modified[2] residual block [12], which contains two convolutional (conv) layers (with batch normalization (BN) [14] and ReLU). The stretching layer serves to change feature map size and dimension. It simply contains an scale-2 nearest up-sampling layer followed by a conv layer with BN+ReLU. The linear compression layer is a single conv layer followed by a Tanh to directly compress feature maps to the RGB space (as side outputs). We prevent any non-linear function in the compression layer that could impede the gradient signals. Starting from a $1024\times4\times4$ embedding, which is computed by CA and a trained embedding matrix, the generator simply uses $M$ $K$-repeat res-blocks connected by $M-1$ in-between stretching layers until the feature maps reach to the targeting resolution. For example, for $256\times256$ resolution and $K=1$, there are $M=6$ 1-repeat res-blocks and 5 stretching layers. With a pre-defined side-output position at scales $\{1,...,s\}$, we apply the compression layer at those positions to generate side output images.

[1]The objective of the generator is omitted as it can be easily inferred.

[2]We remove ReLU after the skip-addition of each residual block, with an intention to reduce sparse gradients.

**Discriminator** The discriminator simply contains consecutive stride-2 conv layers with BN and LeakyReLU. There are two branches are added on the upper layer for the proposed functional discriminator design. One branch is a direct fully convolutional layers to produce a $R \times R$ probability map (see Figure 3) and classify each location as real or fake. Another branch first concatenates the $512 \times 4 \times 4$ feature map and a $128 \times 4 \times 4$ text embedding (replicated by a reduced 128-d text embedding). Then we use an $1 \times 1$ conv to fuse text and image information and a $4 \times 4$ conv layer to classify the image-text pair to real or fake.

The training is similar with the standard alternative training strategy in GANs. Please refer to the supplementary material for training and more network details.

## 4. Experiments

We denote our method as **HDGAN**, referring as High-Definition results and the idea of Hierarchically-nested Discriminators.

**Dataset** We test on three widely used datasets. The CUB dataset [39] contains 11,788 bird images belonging to 200 different categories. The Oxford-102 dataset [29] contains 8189 flow images in 102 different categories. Each image in both datasets is annotated with 10 text descriptions provided by [33]. We pre-process and split the images of CUB and Oxford-102 following the same pipeline in [33, 42]. In the COCO dataset [23], there are 80k training images and 40k validation images. Each image has 5 text descriptions. We use the pre-trained text encoder model provided in [33] to encode each text description into a 1024 embedding vector.

**Evaluation metric** We use three different quantitative metrics to evaluate our method. 1) Inception score [36] is a measurement of both objectiveness and diversity of generated images, it is closely correlated with human judgment on the image quality. For CUB and Oxford-102, we use the fine-tuned inception model provided by StackGAN. For COCO, we directly use the model pre-trained on ImageNet. 2) Multi-scale structural similarity (MS-SSIM) metric [36] is used for further validation. It tests pair-wise variation of generated outputs and can find mode collapses reliably [30]. Lower score indicates higher diversity of generated images (i.e. less model collapses).

3) **Visual-semantic similarity** The aforementioned metrics are widely used for general GANs. The problem of them is that they can not measure the alignment between the generated images and conditioned text. We introduce a new qualitative measurement, namely visual-semantic similarity (VS similarity) inspired by [20]. Denote $\boldsymbol{v}$ as the image feature vector extracted by a pre-trained Inception model $f_{cnn}$[38]. We define a scoring function $c(\boldsymbol{x}, \boldsymbol{y}) = \frac{\boldsymbol{x} \cdot \boldsymbol{y}}{||\boldsymbol{x}|| \cdot ||\boldsymbol{y}||}$. Then, we learn two mapping functions $f_v$ and $f_t$, which map both image and sentence embeddings into a common space in $\mathbb{R}^{512}$, by minimizing the following bi-directional ranking loss:

$$\sum_{\boldsymbol{v}} \sum_{\boldsymbol{t}_{\overline{v}}} \max(0, \delta - c(f_v(\boldsymbol{v}), f_t(\boldsymbol{t}_v)) + c(f_v(\boldsymbol{v}), f_t(\boldsymbol{t}_{\overline{v}}))) + \sum_{\boldsymbol{t}} \sum_{\boldsymbol{v}_{\overline{t}}} \max(0, \delta - c(f_t(\boldsymbol{t}), f_v(\boldsymbol{v}_v)) + c(f_t(\boldsymbol{t}), f_v(\boldsymbol{v}_{\overline{t}}))) \quad (5)$$

where $\delta$ is the margin, which is set as 0.2. $\{\boldsymbol{v}, \boldsymbol{t}\}$ is a ground truth image text pair, and $\{\boldsymbol{v}, \boldsymbol{t}_{\overline{v}}\}$ and $\{\boldsymbol{v}_{\overline{t}}, \boldsymbol{t}\}$ denote mismatched image-text pairs. In the testing stage, given an text embedding $\boldsymbol{t}$, and the generated image $\boldsymbol{x}$, the VS score is calculated as $c(f_{cnn}(\boldsymbol{x}), \boldsymbol{t})$. Higher score indicates better semantic consistency, i.e. stronger alignment between generated images and conditioned text.

| Method | Dataset | | |
|---|---|---|---|
| | CUB | Oxford-102 | COCO |
| GAN-INT-CLS | 2.88±.04 | 2.66±.03 | 7.88±.07 |
| GAWWN | 3.60±.07 | - | - |
| StackGAN | 3.70±.04 | 3.20±.01 | 8.45±.03* |
| StackGAN++ | 3.84±.06 | - | - |
| TAC-GAN | - | 3.45±.05 | - |
| HDGAN | **4.15±.05** | **3.45±.07** | **11.86±.18** |

*Recently, it updated to 10.62±.19 in its source code.

Table 1: The inception-score evaluation on three datasets. The higher score reflects more meaningful synthetic images and higher diversity. The proposed HDGAN outperforms others significantly.

| Method | Dataset | | |
|---|---|---|---|
| | CUB | Oxford-102 | COCO |
| Ground Truth | .302±.151 | .336±.138 | .426±.157 |
| StackGAN | .228±.162 | .278±.134 | −±− |
| HDGAN | **.246±.157** | **.296±.131** | **.199±.183** |

Table 2: The VS similarity evaluation on the three datasets. The higher score represents higher semantic consistency between the generated images and the text information. The groundtruth score is shown in the first row.

### 4.1. Comparative Results

To validate our proposed HDGAN, we compare our results with GAN-INT-CLS [33], GAWWN [34], TAC-GAN [6], StackGAN [42] and also its improved version StackGAN++ [43], and Progressive GAN [17][3]. We especially compare with the current state of the art, StackGAN (results are obtained from its provided models).

Table 1 shows the quantitative inception-score evaluation. We follow StackGAN' experiment setting to sample $\sim 30,000$ $256^2$ images for evaluation. HDGAN achieves

[3]StackGAN++ and Prog.GAN are two very recently released preprints we noticed. We acknowledge them as they also target at generating high-resolution images.


Figure 4: The generated images on CUB compared with StackGAN. Each sample shows the input text and generated $64^2$ (left) and $256^2$ (right) images. Our results have significantly higher quality and preserve more semantic details, for example, "the brown and white feathers and read head" in the last column is much better reflected in our images. Moreover, we observed our birds exhibit richer poses (e.g. the frontal/back views in the second/forth columns).

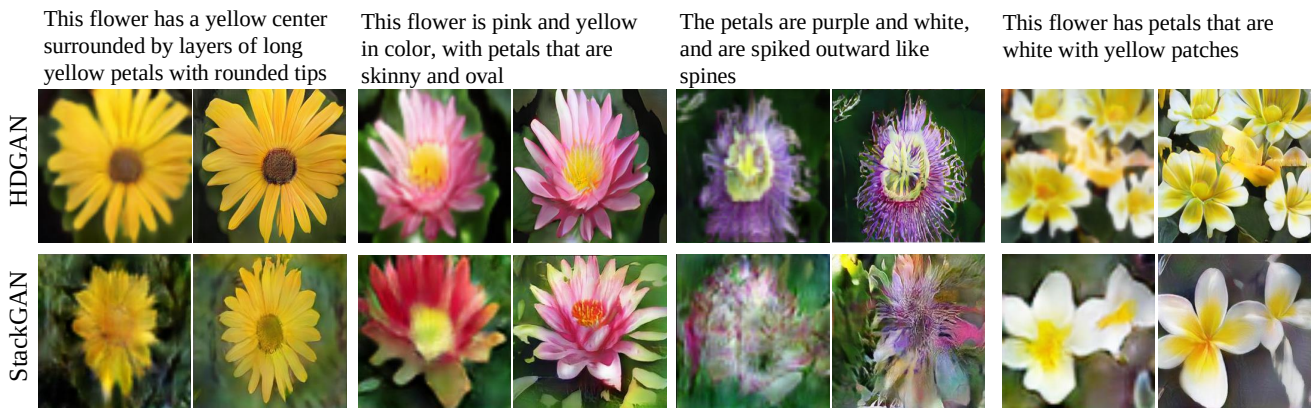


Figure 5: The generated images on Oxford-102 compared with StackGAN. Our generated images perform more natural satisfiability and higher contrast and can generate complex flower structures (e.g. spiked petals) like the third example.

significantly improvement compared against other methods. For example, it improves StackGAN by .45 and StackGAN++ by .31 on CUB. HDGAN achieves competitive results with TAC-GAN on Oxford-102. TAC-GAN uses image labels to increase the discriminability of generators, while we do not use any extra knowledge. Figure 4 and Figure 5 compare the qualitative results with StackGAN, by demonstrating more semantics details, richer poses, and more complex generated structures, which strongly prove the superiority of HDGAN. Moreover, we qualitatively compare the diversity of samples conditioned on the same text (with different input noises) in Figure 6 left. HDGAN can generate obviously more successful samples. Please refer to the supplementary material for more results.

Table 2 compares the VS results on the three datasets. The results of the ground truth image-text pair are shown for reference. HDGAN achieves consistently better performance on both CUB and Oxford-102. This results demonstrate that HDGAN can better capture the visual semantic information in generated images.

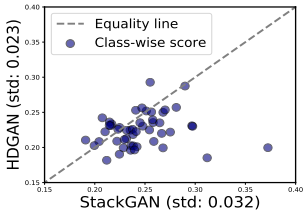


| Method | MS-SSMI |
|---|---|
| StackGAN | 0.234 |
| Prog.GAN | 0.225 |
| HDGAN | **0.215** |

Table 3: Left: Class-wise MS-SSMI evaluation. Lower score indicates higher intraclass dissimilarity. The points below the equality line represent classes our HDGAN wins. The inter-class std is shown in axis text. Right: Overall (not class-wised) MS-SSMI evaluation.

Table 3 compares the MS-SSMI image quality evaluation score with StackGAN and Prog.GAN for bird image generation. StackGAN and our HDGAN use text as input so the generated images are separable in class. We randomly sample $\sim 20,000$ image pairs (400 per class) and show the class-wise score in the left figure. HDGAN outperforms StackGAN in majority of classes and also has

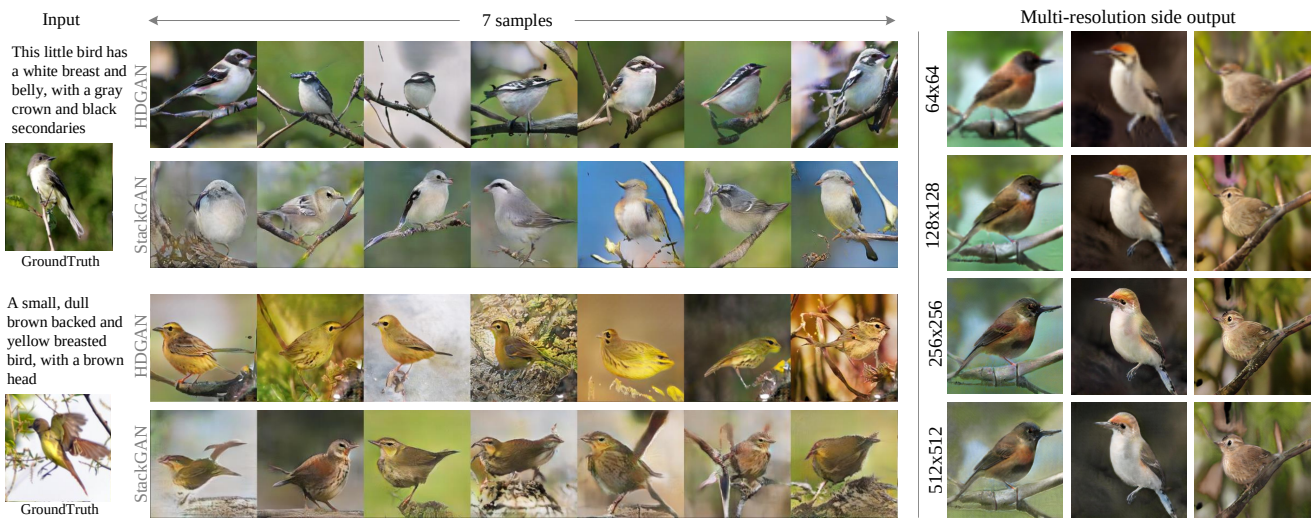


Figure 6: Left: Diverse samples are shown given a single input text. The proposed HDGAN (top) show obviously more details and higher diversity. Right: Side outputs of HDGAN with increasing resolutions. Different resolutions are semantically consistent and semantic details appear as the resolution increases.

lower inter-class standard deviation (.023 vs. .032). Note that Prog.GAN uses noise input rather than text. We can compare with it for the general measure of image diversity. Following the procedure of Prog.GAN, we randomly sample $\sim 10,000$ image pairs from all generated samples (We use $256^2$ images provided by Prog.GAN) and show the results in Table 3 right. HDGAN outperforms both methods.

The right figure compares the multi-resolution inception score on CUB. Our results are from the side outputs of a single model. As can be observed, our $64^2$ results outperform the $128^2$ results of StackGAN and our $128^2$ results also outperform $256^2$ results of StackGAN substantially. It strongly demonstrates our HDGAN better preserves semantically consistent information in all resolutions. Figure 6 right qualitatively validate this property. However, we observed that, in StackGAN, the low-resolution images and high-resolution images sometimes are visually inconsistent (see examples in Figure 4 and Figure 5).

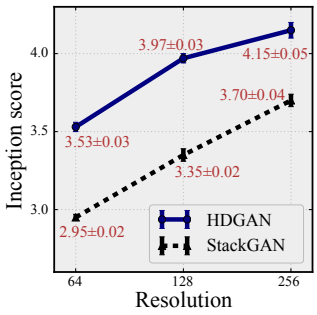


## 4.2. Style Transfer Using Sentence Interpolation

Ideally, a well trained model should learn a smooth linear latent manifold of the images. To demonstrate this ability of HDGAN, we generate images using the linearly interpolated embeddings between a source sentence and a target sentence. As shown in Figure 7, the generated images show smooth style transformation and well reflect the semantic details in sentences. In the first row, the generated birds gradually turn the color from yellow to brown. In the second row, two sentences with more complicated appearance descriptions is used, we can see that our model successfully captures these subtle features and tune the bird appearance gradually.

## 4.3. On the effects of Individual Components

**Hierarchically-nested adversarial training** Our hierarchically-nested discriminators play a role of regularizing the layer representations (at scale $\{64, 128, 256\}$). In Table 4, we compare the performance of HDGAN by removing part of discriminators on both CUB and COCO datasets. As can be seen, increasing the usage of discriminators at different scales have positive effects. And using discriminators at $64^2$ is critical (by comparing 64-256 and 128-256 cases). For now, we are unsure if adding more discriminators and even on lower resolution would be helpful. Further validation will be conducted. StackGAN emphasizes the importance of using text embeddings not only at input but also with intermediate features of the generator, by showing a large drop from 3.7 to 3.45 without doing so. While our method only uses text embeddings at the input. Our significantly improved results demonstrate the effectiveness of our hierarchically-nested adversarial training to maintain such semantic information and high inception score.

**On the Local Image Loss** We also study the effectiveness of the proposed local adversarial image loss. Table 4 compares the case by removing the local loss (denoted as 'w/o local'). Besides, the local image loss also helps improve the visual-semantic matching evidenced by the higher VS score of 'w/ local'. We hypothesis that it is because adding the separate local image loss can offer the pair loss

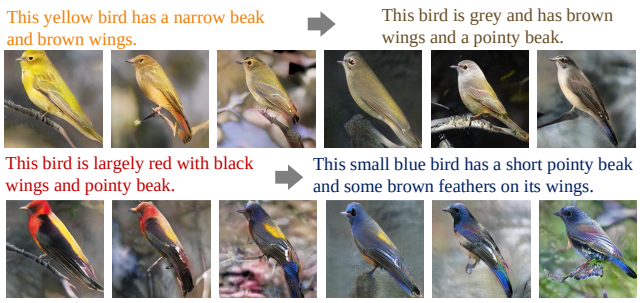


Figure 7: Text embedding interpolation from the source to target sentence results in smooth image style changes to match the targeting sentence.

| Components | | | Inception score | |
|---|---|---|---|---|
| 64 | 128 | 256 | CUB | COCO |
| | | ✓ | 3.52±.04 | - |
| | ✓ | ✓ | 3.99±.04 | - |
| ✓ | | ✓ | 4.14±.03 | 11.29±.18 |
| ✓ | ✓ | ✓ | 4.15±.05 | 11.86±.18 |

Table 4: Ablation study of hierarchically-nested adversarial discriminators on CUB and COO. ✓ indicates whether a discriminator at a certain scale is used. See text for detailed explanation.

| | Inc. score | VS |
|---|---|---|
| w/o local image loss | 3.12±.02 | .263±.130 |
| w/ local image loss | 3.45±.07 | .296±.130 |

Table 5: Ablation study on the local adversarial loss. See text for detailed explanation.

more "focus" on learning the semantic consistency. Furthermore, we also quantitatively compare the generated results in Figure 8. Although both models can successfully capture the semantic details in text, the model with the local loss more precisely generate object structures described in conditioned text.

**Design principles** StackGAN shows the failure of directly training a vanilla 256×256 GAN to generate meaningful images. We test this extreme case using our method by removing all nested discriminators (the first row of Table 4). Our method still generates fairly good results, which demonstrate the effectiveness of our design framework (see Section 3.4).

Initially, we tried to share the top layers of the hierarchical-nested discriminators of HDGAN inspired by [24]. The intuition is that all discriminators have a common goal to differentiate real and fake despite difficult scales and such sharing would reduce their inter-variances. However, we did not observe benefits from this mechanism and our independent discriminators can be trained very stably.

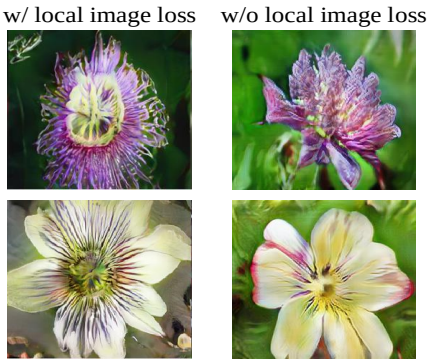


Figure 8: Qualitative evaluation of the local adversarial loss. We can see the two images w/ the local image loss more accurately exhibit complex flower petal structures described in the (colored) text.

## 5. Conclusion

In this paper, we present a novel and effective method to tackle the problem of generating images conditioned on text descriptions. We present a new dimension of playing adversarial games along the depth of the generator using the hierarchical-nested adversarial objectives, which regularizes the mid-level representations with multi-purpose adversarial losses and help the generator to generate high-resolution photographic images. We also introduce a new evaluation metric to evaluate the semantic consistency between generated images and conditioned text. Extensive experiment results demonstrate that our method, namely HDGAN, performs significantly better than existing state of the arts on three public datasets.

## References

[1] M. Arjovsky, S. Chintala, and L. Bottou. Wasserstein gan. *arXiv preprint arXiv:1701.07875*, 2017. 2

[2] D. Berthelot, T. Schumm, and L. Metz. Began: Boundary equilibrium generative adversarial networks. *arXiv preprint arXiv:1703.10717*, 2017. 2

[3] Z. Cai, Q. Fan, R. S. Feris, and N. Vasconcelos. A unified multi-scale deep convolutional neural network for fast object detection. In *ECCV*, pages 354–370. Springer, 2016. 2

[4] Q. Chen and V. Koltun. Photographic image synthesis with cascaded refinement networks. *ICCV*, 2017. 2

[5] P. Costa, A. Galdran, M. I. Meyer, M. D. Abràmoff, M. Niemeijer, A. M. Mendonça, and A. Campilho. Towards adversarial retinal image synthesis. *arXiv preprint arXiv:1701.08974*, 2017. 2

[6] A. Dash, J. C. B. Gamboa, S. Ahmed, M. Z. Afzal, and M. Liwicki. Tac-gan-text conditioned auxiliary classifier generative adversarial network. *arXiv preprint arXiv:1703.06412*, 2017. 2, 5

[7] E. L. Denton, S. Chintala, R. Fergus, et al. Deep generative image models using a laplacian pyramid of adversarial networks. In *NIPS*, pages 1486–1494, 2015. 2, 3

[8] H. Dong, S. Yu, C. Wu, and Y. Guo. Semantic image synthesis via adversarial learning. *ICCV*, 2017. 1, 2

[9] A. Dosovitskiy and T. Brox. Generating images with perceptual similarity metrics based on deep networks. In *NIPS*, 2016. 2

[10] I. Durugkar, I. Gemp, and S. Mahadevan. Generative multi-adversarial networks. *arXiv preprint arXiv:1611.01673*, 2016. 2, 3

[11] I. Goodfellow, J. Pouget-Abadie, M. Mirza, B. Xu, D. Warde-Farley, S. Ozair, A. Courville, and Y. Bengio. Generative adversarial nets. In *NIPS*, 2014. 2, 3

[12] K. He, X. Zhang, S. Ren, and J. Sun. Identity mappings in deep residual networks. In *ECCV*, 2016. 4

[13] X. Huang, Y. Li, O. Poursaeed, J. Hopcroft, and S. Belongie. Stacked generative adversarial networks. *CVPR*, 2017. 2, 3

[14] S. Ioffe and C. Szegedy. Batch normalization: Accelerating deep network training by reducing internal covariate shift. In *ICML*, 2015. 4

[15] P. Isola, J.-Y. Zhu, T. Zhou, and A. A. Efros. Image-to-image translation with conditional adversarial networks. *CVPR*, 2017. 1, 2

[16] J. Johnson, A. Alahi, and L. Fei-Fei. Perceptual losses for real-time style transfer and super-resolution. In *ECCV*, 2016. 2

[17] T. Karras, T. Aila, S. Laine, and J. Lehtinen. Progressive growing of gans for improved quality, stability, and variation. In *arXiv preprint arXiv:1710.10196*, 2016. 2, 3, 5

[18] D. P. Kingma and M. Welling. Auto-encoding variational bayes. *arXiv preprint arXiv:1312.6114*, 2013. 2

[19] D. P. Kingma and M. Welling. Auto-encoding variational bayes. *ICLR*, 2013. 4

[20] R. Kiros, R. Salakhutdinov, and R. S. Zemel. Unifying visual-semantic embeddings with multimodal neural language models. *arXiv preprint arXiv:1411.2539*, 2014. 5

[21] C. Ledig, L. Theis, F. Huszár, J. Caballero, A. Cunningham, A. Acosta, A. Aitken, A. Tejani, J. Totz, Z. Wang, et al. Photo-realistic single image super-resolution using a generative adversarial network. *CVPR*, 2017. 2

[22] C.-Y. Lee, S. Xie, P. Gallagher, Z. Zhang, and Z. Tu. Deeply-supervised nets. In *AIS*, 2015. 2

[23] T.-Y. Lin, M. Maire, S. Belongie, J. Hays, P. Perona, D. Ramanan, P. Dollár, and C. L. Zitnick. Microsoft coco: Common objects in context. In *ECCV*, 2014. 2, 5

[24] M.-Y. Liu, T. Breuel, and J. Kautz. Unsupervised image-to-image translation networks. *arXiv preprint arXiv:1703.00848*, 2017. 8

[25] J. Long, E. Shelhamer, and T. Darrell. Fully convolutional networks for semantic segmentation. In *CVPR*, 2015. 2

[26] L. Metz, B. Poole, D. Pfau, and J. Sohl-Dickstein. Unrolled generative adversarial networks. *arXiv preprint arXiv:1611.02163*, 2016. 2

[27] H. T. K. Miriam Cha, Youngjune Gwon. Adversarial nets with perceptual losses for text-to-image synthesis. *arXiv preprint arXiv:1708.09321*, 2017. 2

[28] T. D. Nguyen, T. Le, H. Vu, and D. Phung. Dual discriminator generative adversarial nets. In *NIPS*, 2017. 3

[29] M.-E. Nilsback and A. Zisserman. Automated flower classification over a large number of classes. In *ICCVGIP*, 2008. 2, 5

[30] A. Odena, C. Olah, and J. Shlens. Conditional image synthesis with auxiliary classifier gans. *arXiv preprint arXiv:1610.09585*, 2016. 2, 5

[31] A. v. d. Oord, N. Kalchbrenner, and K. Kavukcuoglu. Pixel recurrent neural networks. *ICML*, 2016. 2

[32] A. Radford, L. Metz, and S. Chintala. Unsupervised representation learning with deep convolutional generative adversarial networks. *arXiv preprint arXiv:1511.06434*, 2015. 2

[33] S. Reed, Z. Akata, X. Yan, L. Logeswaran, B. Schiele, and H. Lee. Generative adversarial text to image synthesis. *ICML*, 2016. 1, 2, 3, 5

[34] S. E. Reed, Z. Akata, S. Mohan, S. Tenka, B. Schiele, and H. Lee. Learning what and where to draw. In *NIPS*, 2016. 2, 5

[35] T. Salimans, I. Goodfellow, W. Zaremba, V. Cheung, A. Radford, and X. Chen. Improved techniques for training gans. In *NIPS*, 2016. 2

[36] T. Salimans, I. Goodfellow, W. Zaremba, V. Cheung, A. Radford, X. Chen, and X. Chen. Improved techniques for training gans. In *NIPS*. 2016. 2, 5

[37] A. Shrivastava, T. Pfister, O. Tuzel, J. Susskind, W. Wang, and R. Webb. Learning from simulated and unsupervised images through adversarial training. *CVPR*, 2017. 2, 4

[38] C. Szegedy, W. Liu, Y. Jia, P. Sermanet, S. Reed, D. Anguelov, D. Erhan, V. Vanhoucke, and A. Rabinovich. Going deeper with convolutions. In *CVPR*, June 2015. 5

[39] P. Welinder, S. Branson, T. Mita, C. Wah, F. Schroff, S. Belongie, and P. Perona. Caltech-ucsd birds 200. 2010. 2, 5

[40] S. Xie and Z. Tu. Holistically-nested edge detection. In *ICCV*, 2015. 2

[41] J. Yang, A. Kannan, D. Batra, and D. Parikh. Lr-gan: Layered recursive generative adversarial networks for image generation. *arXiv preprint arXiv:1703.01560*, 2017. 2

[42] H. Zhang, T. Xu, H. Li, S. Zhang, X. Wang, X. Huang, and D. Metaxas. Stackgan: Text to photo-realistic image synthesis with stacked generative adversarial networks. In *ICCV*, 2017. 1, 2, 3, 4, 5

[43] H. Zhang, T. Xu, H. Li, S. Zhang, X. Wang, X. Huang, and D. Metaxas. Stackgan++: Text to photo-realistic image synthesis with stacked generative adversarial networks. In *arXiv preprint arXiv:1710.10916*, 2017. 5

[44] J.-Y. Zhu, T. Park, P. Isola, and A. A. Efros. Unpaired image-to-image translation using cycle-consistent adversarial networks. *ICCV*, 2017. 2, 4